/
Article / Book Information

Title	Development of New Terminal Fixation Method for Synthetic Fiber Ropes
Authors	Atsushi Horigome, Gen Endo, Atsushi Takata, Youki Wakabayashi
Citation	IEEE Robotics and Automation Letters, Vol. 3, Issue 4, pp. 4321-4328
Pub. date	2018, 6
Copyright	(c) 2018 IEEE. Personal use of this material is permitted. Permission from IEEE must be obtained for all other uses, in any current or future media, including reprinting/republishing this material for advertising or promotional purposes, creating new collective works, for resale or redistribution to servers or lists, or reuse of any copyrighted component of this work in other works.
DOI	https://dx.doi.org/10.1109/LRA.2018.2851033
Note	This file is author (final) version.

Development of New Terminal Fixation Method for Synthetic Fiber Ropes

Atsushi Horigome[1], Gen Endo[1], Atsushi Takata[1], and Youki Wakabayashi[1]

Abstract—A synthetic fiber rope is potentially capable of replacing a stainless steel wire rope because it is light weight, and has high tensile strength and flexibility. In order to exploit the maximum tensile strength of the rope, a terminal fixation method with a sufficient fixing force is essential. However, this is extremely difficult in the case of synthetic fiber ropes due to their small friction coefficients. This paper proposes a new terminal fixation method combined with a grooved pulley and pin. The grooved pulley is utilized in order to increase the friction between the synthetic fiber rope and the pulley, and the rope is wound around the grooved pulley. The extremity of the rope is fixed at a pin by hanging a loop with a figure-eight knot. The appropriate groove shape is found experimentally and it is confirmed that our method achieves maximum fixation force of 91.3% against the rope breaking force. We provide implementations examples for a long-reach tendon-driven manipulator.

Index Terms—Tendon/Wire Mechanism, Synthetic Fiber Ropes, Terminal Fixation, Mechanism Design

I. INTRODUCTION

HIGH performance synthetic fiber ropes are attracting the attention of many researchers in the field of robotics due to their tensile strengths being the same or larger to those of a stainless steel wire rope, whereas their density is only 1/5 to 1/8, in comparison to stainless steel wire ropes. Moreover, synthetic fiber ropes are very flexible and easy to bend; thus, it is possible to design more compact tendon-driven robots. For example, synthetic fiber ropes were introduced as essential mechanical components for achieving a compact dexterous robotic hand [1] [2]. The humanoid robot Kenshiro [3] and our quadruped robot TITAN-XIII [4] also used synthetic fiber ropes in order to drive articulated limbs. Synthetic fiber ropes have also been used in order to generate large contracting forces for artificial muscles [5], while reducing the total weight of the muscle. We also proposed a coupled tendon-driven 3D multi-joint manipulator by using synthetic fiber ropes [6] in order to achieve a very long cantilever structure for a decommissioning task, as shown in Fig. 1. However, the development of a tendon-driven robot using synthetic fiber ropes faces a practical problem: there is no mechanical design guideline for synthetic fiber ropes. In most cases, the manufacturer only provides the tensile strength of the rope,

[1]All authors are with the Department of Mechanical and Aerospace Engineering, Tokyo Institute of Technology , 2-12-1 Ookayama, Meguro-ku, Tokyo, 152-8552, Japan gendo@mes.titech.ac.jp
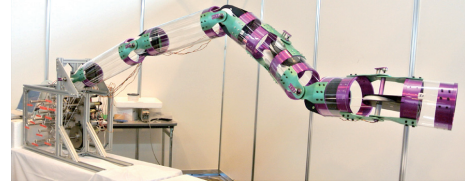
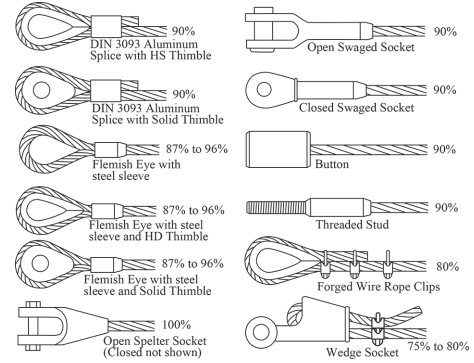Fig. 1: Coupled tendon-driven 3D multi-joint manipulator.

Fig. 2: Terminal fixation methods for steel wire ropes (modified based on data from [11].

while the other mechanical properties of the rope remain unknown. In the literature, several mechanical properties of synthetic fiber ropes have been investigated [7] [8]. However, their main applications were tether moorings as a marine rope, and required performance and specifications that were completely different to a tendon-driven robot. Although some robotics researchers have studied the physical properties of synthetic fiber rope [9] [10], to the best of our knowledge, there has been no comprehensive study that has provided a systematic design guideline.

In this study, our ultimate goal was to establish a design guideline for using synthetic fiber ropes for a tendon-driven robot. This guideline should include various mechanical properties such as elongation, creeping, frequency response, endurance against repetitive bending, and so on.

In this particular article, we focused on terminal fixation methods for synthetic fiber ropes. Fixing the end of a synthetic fiber rope is very difficult due to the very small friction coefficients, in comparison to a metal wire rope. For example, based on our preliminary experiments, the coefficient of static friction of the synthetic fiber rope covered with an ultra-high molecular weight polyethylene (UHPE) fiber sleeve was 0.0438, whereas, that of the stainless wire rope was 0.237. Therefore, synthetic fiber rope tends to slip off the fixing parts before reaching the maximum tensile force. Thus, the maximum strength of synthetic fiber ropes has not yet been
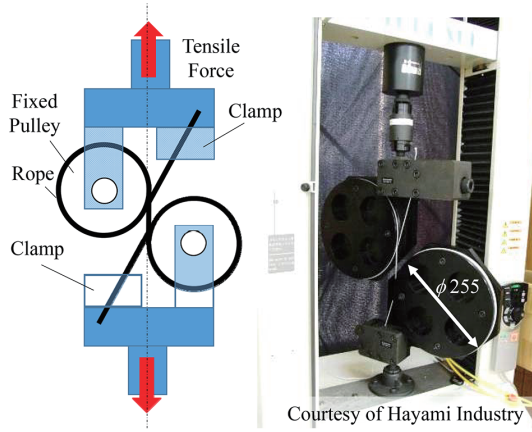
Fig. 3: The measurement apparatus of the synthetic fiber rope breaking strength.

fully exploited, due to the absence of tight terminal fixation methods.

In the case of steel wire ropes, various terminal fixation methods have been already developed. Their strength efficiencies (defined as the terminal fixing force divided by the breaking tensile force) were measured quantitatively (Fig. 2) [11], and it was found that some fixation methods had a strength efficiency of 95-100%, which suggests mature fixation methodologies.

On the contrary, in the case of synthetic fiber ropes, the terminal fixation method has not been fully established yet, and ad-hoc solutions have been frequently applied based on technical know-how. [12] proposed a terminal fixation by using stainless steel cylinders with tapered holes. However, its strength efficiency was only 32%. Figure 3 shows the experimental apparatus of a rope manufacturer for measuring the breaking force of the synthetic fiber rope. To tightly fix the extremities of the rope, very large fixed pulleys were used to reduce the tensile force by belt friction, equipped with very large. Even if the manufacturer used this large apparatus, the maximum breaking force would be occasionally unavailable due to fixation slippage. Moreover, this fixation method is too large for a robot to be installed.

In our previous work, we experimentally evaluated several terminal fixation methods with an adjustable length function. However, the maximum strength efficiency still remained at 83.7% [13], which is not so high when compared to the steel wire rope fixation.

In this article, our goal was to establish a length-adjustable compact fixation method for a synthetic fiber rope that could achieve a strength efficiency larger than 90%. We propose a new terminal fixation method combined with a grooved pulley and pin. The grooved pulley was utilized in order to increase the friction between the synthetic fiber rope and pulley. The rope was wound around the pulley, and the rope extremity was fixed at the pin by hanging a loop with a knot.

The rest of this paper is organized as follows. Section II briefly reviews our previous work. Section III propose a new fixation method composed of a grooved pulley and pin. Section IV discusses the design of the grooved pulley. In Section V we describe how the appropriate shape of the groove was obtained experimentally. Section VI describes
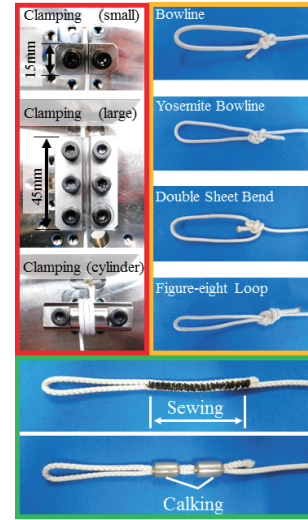

Fig. 4: Conventional terminal fixations for synthetic fiber ropes.
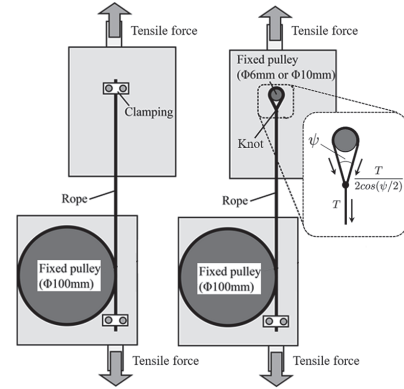

Fig. 5: Measurement of terminal fixation force.

the implementation examples for a long-reach tendon-driven manipulator. Section VII concludes this paper and discusses future work.

II. EXPERIMENTAL EVALUATIONS OF CONVENTIONAL TERMINAL FIXATION METHODS

To the best of our knowledge, there has been no comprehensive discussion of terminal fixation methods for synthetic fiber ropes. Thus, we started with the experimental evaluations of conventional methods.

In our previous work [13], we measured the fixing forces for three types of fixations, as shown in Fig.4. The first type was the clamping in Fig. 4 (surrounded by a red square). The fixation force was generated by the friction force between the rope and clamping block. The friction force could be increased by a higher fixing bolt tightening torque, and/or lager length of the clamping block. The clamping of the cylinder was our original method of exploiting the additional belt friction. The second type was to make a loop with a knot, as shown in Fig. 4 (surrounded by an orange square). The loop is hanged on a pin. We evaluated four kinds of knots which have been commonly used in rope work in order to achieve a high tightening force. The third type was special termination processes by the rope manufacturer, as shown in Fig. 4 (surrounded by a green

square). The length of sewing or number of calkings can be ordered, and the rope manufacturer processes the termination.

The fixing force was measured by a tensile force testing device (AG-I, Shimadzu, maximum testing tension:100 kN) with jigs, as shown in Fig. 5. The tested fixation was installed on the upper jig, and the rope was wound around sufficiently large pulleys with a sufficient number of turns in order to reduce the tension of the rope on the lower jig. Two synthetic fiber ropes (Dyneema1 and Zylon3), and one stainless wire rope (Stainless3) were tested. The specifications for each rope are shown in Table II.

Table I shows the strength efficiency of each fixation method. In the case of Stainless3, conventional clamping achieved 80-90%; however, in the case of synthetic fiber ropes, their strength efficiencies were smaller than 75%. Our original cylinder clamp with eight turns for Zylon3 performed the maximum value of 83.7%. However, it was not effective for Dyneema1, whose maximum value was 58.9%. In the case of Dyneema1, the optimum number of turns was four, while more than four turns were not effective due to the distribution of the clamping force in each turn, which results in rope slippage and frictional wear [13]. With regard to knotting with a sufficiently small loop angle ψ, the fixation force ranged from 36.6 to 53.2%, and the loop made by the figure-eight knot performed the strongest fixation. Rope breaking always occurs at the knot, due to sharp bending. The special termination processes, namely, calking and sewing, could achieve highest strength efficiency if they had sufficient length for the processes. However, these special processes have the serious drawback of requiring to specify the length of the synthetic fiber rope, when the process is ordered. It is very difficult and not practical to specify the total length of the rope in advance when the rope is applied to a tendon-driven robot. Moreover, under static loading, the synthetic fiber ropes often exhibit creeping. Thus, it is desirable for the terminal fixation method to possess a function for adjusting the rope length.

The results are summarized as follows.

- Simple clamping was insufficient for synthetic fiber rope fixation.
- Loop fixation with a figure-eight knot achieved a strength

TABLE I: Strength efficiency of various end fixations [13].

		Dyneema1	Zylon3	Stainless3
Diameter	[mm]	2	2	2
Tensile strength	[kN]	2.14	2.99	3.50
Clamping (small)	[%]	28.3	18.6	80.0
Clamping (small)*	[%]	42.9	37.3	-
Clamping (large)	[%]	65.0	72.3	90.2
Clamping (cylinder)	[%]	58.9	83.7	-
Bowline	[%]	47.1	36.6	63.1
Yosemite bowline	[%]	51.2	45.9	-
Double sheet bend	[%]	50.5	46.5	-
Figure-eight loop	[%]	50.9	53.2	73.6
Calking (1)	[%]	58.9	23.9	-
Calking (2)	[%]	89.6	47.8	-
Calking (3)	[%]	83.1	79.2	-
Sewing (10 mm)	[%]	48.8	34.1	-
Sewing (25 mm)	[%]	85.4	73.5	-
Sewing (40 mm)	[%]	81.3	90.8	-

*Making knot at the end of clamping in order to prevent slipping.

▇ : Slipping   ☐ : Rope breaking

efficiency of 53.2%.
- Calking and sewing had the highest strength efficiency; however, the length of the rope was fixed.

For more details, see [13].

III. PROPOSAL OF A NEW TERMINAL FIXATION METHOD

In our previous work, there was no fixation method achieving a strength efficiency of 90% for a synthetic fiber rope with an adjustable length function. We proposed a new fixation method by utilizing a grooved pulley and the pin shown in Fig. 6, in order to achieve higher strength efficiency. Our previous work revealed that a loop made by a figure-eight knot and pin could support approximately 50% of the maximum tensile strength. Thus, we needed to decrease the tension of the rope from 100% to 50%, before the figure-eight knot. To achieve this tension reduction, a fixed pulley was installed, and the rope was wrapped around the pulley in order to exploit belt friction. Since the friction coefficient of the synthetic fiber rope was very small, a conventional flat pulley was not appropriate. Therefore, we propose to use a grooved pulley that can increase the friction force according to the wedge effect.

The proposed method has two advantages. (1)The length of the rope is easily adjusted by changing the position of the knot without requiring a special process and/or tools. (2)The grooved pulley makes the fixation parts compact, and minimizes the total length of the rope. If we use a flat pulley, as shown in Fig. 3(right), then, the lower friction coefficient would require a larger wrapped angle. As a result, the pulley width increased and the total length of the rope became longer. A longer rope generates more elongation due to elasticity and creeping, which may cause tension reduction or slack.

IV. DESIGN OF THE GROOVED PULLEY

In this study, our goal was to develop a compact, length adjustable fixation method that achieves a strength efficiency of more than 90%. The target rope diameter was set to 2 mm. There were two important challenges in the design of the grooved pulley in order to achieve a higher fixation force. One was the pulley diameter, and the other was the shape of the groove.
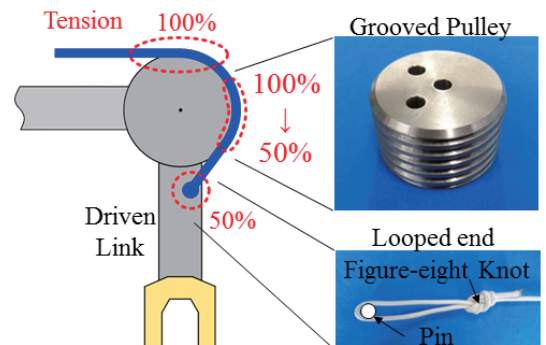

Fig. 6: Schematic image of proposed fixation method.

A. Diameter of the grooved pulley

A smaller pulley allows for a more compact mechanism; however, it is generally known that sharp bending reduces rope strength due to stress distribution in the radial direction of the rope. Thus, there is a trade-off between pulley compactness and strength efficiency.

In our previous work [13], we measured the strength reduction due to static bending by using various flat pulleys with different radii, and obtained the following empirical formula:

$$\eta_b \approx 1 - \frac{0.59}{\sqrt[3]{(D/d)^2}}, \tag{1}$$

where η_b is the strength efficiency due to static bending, D is the pulley diameter, and d is the rope diameter, respectively. This formula is applicable to both a stainless wire rope and a synthetic fiber rope. To achieve $\eta_b > 0.9$, the pulley diameter should be at least larger than 28.7 mm. Additionally, strength efficiency would decrease due to the stress concentration in the groove. By considering a trade-off between pulley compactness and strength efficiency, as well as ease of prototyping, we chose $D =37.5$ mm where $d = 2.0$ mm and $\eta_b = 0.916 > 0.9$. Additionally, we selected the diameter of the pin as 6 mm in order to achieve $\eta_b = 0.71 > 0.5$.)

B. Shape of the groove

1) Analytical Model: In order to derive the analytical friction force, we introduce a belt friction equation (also known as the capstan equation and Euler-Eytelwein's formula) [14][15]. Figure 7 shows an analytical model of the rope wrapped around a fixed pulley (left), and an infinitesimal rope segment subtended by the angle $\Delta\theta$ (right). Let us consider the forces acting on an infinitesimal rope segment for $\Delta\theta$. When tension T was applied on the left, the tension on the right was changed to $T + \Delta T$ due to friction force F_{fr} between the rope and the pulley. (Here, $T \geq 0$, $\Delta T \leq 0$.) By defining N as a normal reaction force from the pulley, we obtained the following equations by the equilibrium of forces in the x and y directions, respectively.
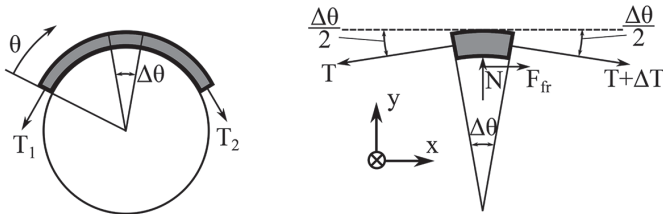
Fig. 7: Analytical model of rope wrapped around a fixed pulley.
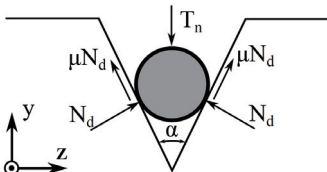
Fig. 8: Equilibrium of forces in the groove

$$F_{fr} + (T + \Delta T) \cos\left(\frac{\Delta\theta}{2}\right) - T \cos\left(\frac{\Delta\theta}{2}\right) = 0. \tag{2}$$

$$N - (T + \Delta T) \sin\left(\frac{\Delta\theta}{2}\right) - T \sin\left(\frac{\Delta\theta}{2}\right) = 0. \tag{3}$$

Here, $\Delta\theta, \Delta T$ can be denoted to $d\theta, dT$, we approximate $\cos\left(\frac{d\theta}{2}\right) \approx 1$, $\sin\left(\frac{d\theta}{2}\right) \approx \frac{d\theta}{2}$. By neglecting the second order term, we obtain:

$$F_{fr} = -dT, \tag{4}$$
$$N = Td\theta. \tag{5}$$

Here, we assume Coulomb friction and define μ as the static friction coefficient; then we obtain:

$$-dT = F_{fr} \leq \mu N = \mu T d\theta. \tag{6}$$

We obtain the following by dividing T and by integrating both sides.

$$-\int_{T_1}^{T_2} \frac{dT}{T} \leq \int_0^{\theta_w} \mu d\theta, \tag{7}$$

$$\frac{T_1}{T_2} \leq \exp\left(\mu\theta_w\right) \tag{8}$$

where θ_w is a wrapped angle. Provided that the maximum static friction acts between the rope and the pulley, the initial tension T_0 acts at the beginning of the wrapping, and θ is the angle measured from the initial wrapping point. Then, the tension T at θ can be expressed as:

$$T = T_0 \exp\left(-\mu\theta\right). \tag{9}$$

According to the above equation, the tension decreases depending only on the coefficient of static friction and wrapped angle, regardless of pulley and rope diameters.

Subsequently, we derived the relationship between rope tension and friction force in the case of the grooved pulley. Figure 8 shows the cross section of the rope in the grooved pulley, and depicts the forces acting on the rope. α is the groove angle, T_n is the force acting in the direction towards the center of the pulley due to rope tension, N_d is the normal reaction force from the groove surface, and μN_d is the reaction force to prevent the rope from moving downward. In this case, the force equilibrium in the z direction was trivial due to the symmetry. We obtained the following equation based on the equilibrium of forces in the y direction.

$$2N_d \sin\left(\frac{\alpha}{2}\right) + 2\mu N_d \cos\left(\frac{\alpha}{2}\right) - T_n = 0. \tag{10}$$

Here, by using Equation(5), $T_n = Td\theta$, we obtain:

$$N_d = \frac{T_n}{2\left(\sin\left(\frac{\alpha}{2}\right) + \mu\cos\left(\frac{\alpha}{2}\right)\right)} = \frac{Td\theta}{2\left(\sin\left(\frac{\alpha}{2}\right) + \mu\cos\left(\frac{\alpha}{2}\right)\right)}. \tag{11}$$

Therefore, we use Equation (4) as follows:

$$-dT \leq \mu(2N_d) = \frac{\mu Td\theta}{\sin\left(\frac{\alpha}{2}\right) + \mu\cos\left(\frac{\alpha}{2}\right)}. \tag{12}$$

By comparing to Equation(6), we can define the equivalent friction coefficient as:

$$\mu' = \frac{\mu}{\sin\left(\frac{\alpha}{2}\right) + \mu\cos\left(\frac{\alpha}{2}\right)}, \tag{13}$$

then, we can express T similar to Equation (9) as:

$$T = T_0 \exp\left(-\mu'\theta\right). \tag{14}$$

The friction force of the grooved pulley can be expressed by the belt friction equation, by replacing the friction coefficient from μ to the equivalent friction coefficient $\mu' = \mu/\left(\sin\left(\frac{\alpha}{2}\right) + \mu\cos\left(\frac{\alpha}{2}\right)\right)$.

Finally, we introduce three-dimensional extended fomulae of the belt friction equation considering spiral pitch p. The rope coils around a cylinder and slides along a spiral path whose pitch is p, as shown in Fig. 9. The reference [16] analytically derive the tension T by using function s, which is the rope length along the spiral path. The solution differs depending on the friction coefficient and spiral geometry. Because a detailed derivation can be found in [16], we only describe the resultant equations here.

$\mu > 2p/\pi D$:

$$T = T_0\left(\frac{k\mu}{2\omega}\sinh\omega s + \cosh\omega s\right)\exp\left(\frac{k\mu}{2}s\right), \tag{15}$$

$\mu = 2p/\pi D$:

$$T = T_0\left(\frac{k\mu}{2}s + 1\right)\exp\left(\frac{k\mu}{2}s\right), \tag{16}$$

$\mu < 2p/\pi D$:

$$T = T_0\left(\frac{k\mu}{2\tilde{\omega}}\sin\tilde{\omega}s + \cos\tilde{\omega}s\right)\exp\left(\frac{k\mu}{2}s\right), \tag{17}$$

where $k = D/2P$, $\omega = \sqrt{Q}/4P$, $\tilde{\omega} = \sqrt{-Q}/4P$, $s = \sqrt{P}\theta$, $P = (D/2)^2 + (p/2\pi)^2$, $Q = (\mu D/2)^2 - (p/\pi)^2$. If $p = 0$, then Eqn. (15) is recovered to Eqn. (9). It is known that increasing the pitch p decreases the ratio of the forces T/T_0; thus, the two-dimensional belt friction equation is representing the upper limit of this ratio. Therefore, p should be minimized as much as possible to maximize the fixing force and achieve compactness.

2) Grooved pulleys tested: The analytical model described in the previous section assumes Coulomb friction and rigid body static kinematics. Under these assumptions, the equivalent friction coefficient depends on α, which can be designed mechanically. However, a synthetic fiber rope was made of soft and deformable material. Thus, the rope may deform along with the grooved shape illustrated in Fig. 10 (left); therefore, it may not satisfy the assumptions made in the analysis. In order to find the appropriate shape of the groove empirically, we set two design parameters, as shown in Fig. 10 (right). α is the angle of the groove and ϕ is the diameter of the fillet
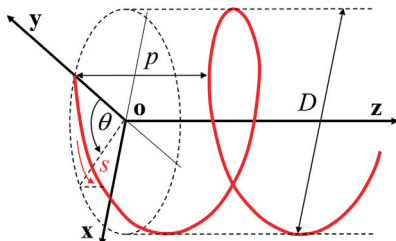
Fig. 9: Rope winding considering pitch effect.

at the bottom of the groove. D and p were set to the constant values of 37.5 mm and 4 mm, respectively. We manufactured nine types of grooved pulleys (combination of $\alpha = 30, 45, 60°$ and $\phi = 0.5, 1.0, 1.5$ mm) made of stainless steel (SUS304). Examples of groove shape with a steel wire rope are depicted in Fig. 11.

V. EXPERIMENTS

A. Ropes used

Table II lists the ropes used to measure the strength efficiencies (except Dyneema1). In particular, Zylon3 was selected in order to find the optimum groove shape. Zylon3 had a two-layer type structure where gently twisted core fibers were covered with braided sleeve fibers in order to prevent the rope surface from wearing. The tensile force was supported only by core fibers, and the sleeve fibers did not contribute towards supporting the tensile force because of the stretchable mesh braiding. Moreover, the core fibers easily slipped against the sleeve fibers contacting the groove surface. Hence, Zylon3 could be considered as the slipperiest rope among the listed ropes. The other three synthetic fiber ropes have an 8-strand
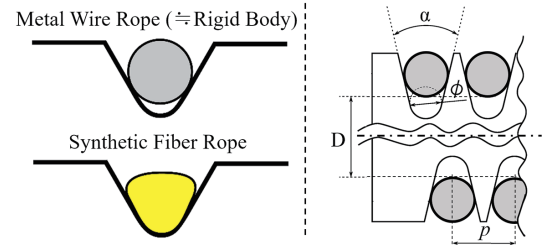

Fig. 10: Rope deformation (left) and design parameters of the grooved pulley (right).
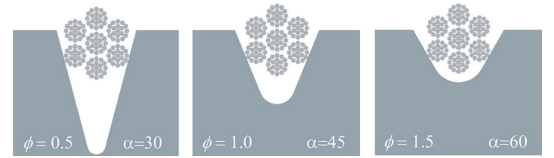

Fig. 11: Examples of groove shape tested.

TABLE II: Ropes used in terminal fixation force measurements. All ropes had diameters of 2 mm.

Name	Model	Supplier	Tensile strength [kN] Measured	Tensile strength [kN] Estimated	%	Weight [g/m]	Core fiber Fiber	Core fiber Structure	Sleeve fiber Fiber	Sleeve fiber Structure
Dyneema1	DB-60	Hayami industry	2.14	3.94	54	1.7	Dyneema® SK-60 UHPE	1760 dtex × 8 strand braid		
Dyneema2	DB-96HSL	Hayami industry	4.29	7.81	54	2.4	Dyneema® SK-71 UHPE	2640 dtex × 8 strand braid		
Zylon2	ZB-308	Hayami industry	6.59	9.89	66	2.9	Zylon® AS PBO	3340 dtex × 8 strand braid		
Zylon3	DY-20ZL	Hayami industry	3.22	3.71	86	2.7	Zylon® AS PBO	10020 dtex	Dyneema® SK-60 UHPE	770dtex × 16 strand braid
Vectran2	VB-308	Hayami industry	4.18	6.41	65	2.9	Vectran® HT Polyarylate	3340 dtex × 8 strand braid		
Stainless3	C-200	Asahi intec	3.50	-		16	SUS304	7×19		

UHPE:ultra high molecular weight polyethylene,
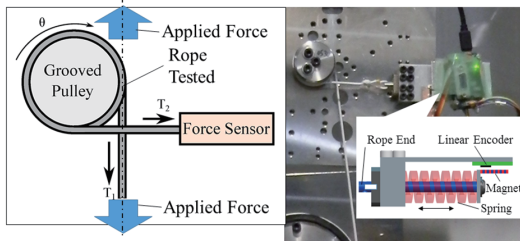PBO: poly(p-phenylene-2,6-benzobisoxazole).

Fig. 12: Tension measurement device.

bladed structure. More detailed physical properties of the synthetic fibers can be found in the Appendix. Stainless3, which represents conventional steel wire ropes, was also tested for the purpose of comparison to Zylon3.

B. Tension Measurement Device

In order to measure the equivalent friction coefficient, both T_1 and T_2 in Fig. 7 were measured. T_1 was measured by the tensile testing machine, and T_2 was measured by a custom-made linear force sensor mounted on the jig shown in Fig. 12. The extremity of the rope was attached to the blue rod, and the rope tension compressed the red spring. The displacement of the rod was measured by a magnetic linear encoder (AS5306, ams), whose positional resolution was 0.015 mm. The maximum load capacity could be adjusted by replacing the coil spring.

C. Results

The strength efficiency for each pulley using Zylon3 and Stainless3 were measured. We set the grooved pulley on the upper jig and the flat pulley with a diameter of 100 mm on the lower jig. The Zylon3 test rope was wound around the grooved pulley, where the contacting angle θ =1350°. In the case of Stainless3, we set θ =270°. The rope was also wound around the lower flat pulley with several turns in order to generate a sufficient fixing force. The time courses of forces, T_1, T_2, were recorded during constant speed stretching until the rope

TABLE III: Experiment condition.

Temperatures	$18.5 - 20.0°\text{C}$
Humidity	$28 - 46\,\%$
Tensile velocity	300 mm/min.
Tension sampling rate	After winding (T_2): 0.015 s Before winding (T_1): 0.01 s

TABLE IV: Average strength efficiency at each groove angle α and each groove fillet diameter ϕ with Zylon3. [%]

		ϕ [mm]		
		0.5	1.0	1.5
α [deg]	30	81.4	86.0	**91.3**
	45	89.8	84.2	89.7
	60	89.6	89.3	88.3

TABLE V: Average strength efficiency at each groove angle α and each groove bottom diameter ϕ with Stainless3. [%]

		ϕ [mm]		
		0.5	1.0	1.5
α [deg]	30	97.5	97.5	97.5
	45	98.5	97.5	98.5
	60	98.5	97.5	98.5

broke. Three trials were conducted and the measured data were averaged. The experimental conditions are listed in Table III.

The experimental results are shown in Table IV and V. In the case of the Zylon3 rope, almost all the grooved pulleys achieved a strength efficiency larger than 85%, and the maximum value was 91.3% where $\alpha = 30, \phi = 1.5$. It is notable that the parameters of ($\alpha = 60, \phi = 0.5$) also had comparable high strength efficiencies, due to this groove shape being almost compatible to the metric screw threads, which can increase its cost efficiency. The maximum value of 91.3% is almost identical to $\eta_b = 0.916$ as we discussed in section IV-A. This suggests that a groove with an appropriate shape does not decrease the tensile strength of the synthetic fiber rope. As we expected, the strength efficiency depended on the groove fillet diameter ϕ, which implied the large deformation of the synthetic fiber rope. On the contrary, there was no significant deviation of strength efficiency with respect to the ϕ change in the case of Stainless3, since the stainless wire rope was hard to deform in the radial direction.

Figures 14 and 13 show the relationship between the groove angle α and the equivalent friction coefficient μ'. In order to derive μ', we numerically solved Eqns. (15)–(17) by replacing μ with μ' and obtained a unique solution. The result is also compared with μ' derived using Eqn. (9). (The values at $\alpha = 180°$ were obtained by using the flat pulleys. Each of the error bars show a standard error for the three samples.) In the case of Stainless3, μ' was increased when α decreased, and its tendency was similar to the theoretical value of Eqn. (13). Moreover, the maximum μ' reached 0.6, which was very large. The difference of μ' due to pitch p was less than 0.9%. Interestingly, the experimental values were higher than the theoretical values. We think that this was due to the surface roughness of Stainless3. In Fig. 10, we assume the cross-section surface of the rope is a circle. However, actual cross-section surface of the Stainless3 rope was like shown in Fig.11.
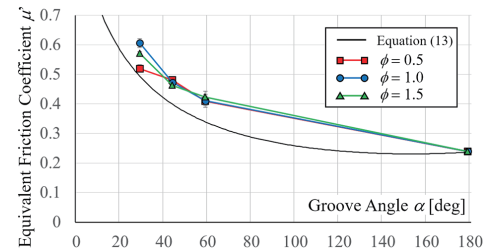
Fig. 13: Relationship between groove angle and equivalent friction coefficient with Stainless3.
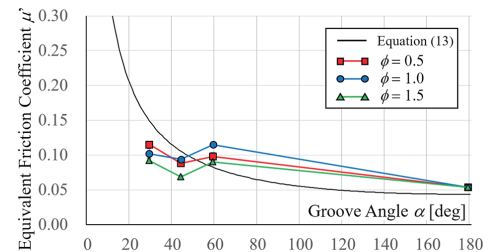
Fig. 14: Relationship between groove angle and equivalent friction coefficient with Zylon3.

The side surface of the rope was jaggy and it might catch the groove stronger. On the contrary, in the case of the Zylon3, μ' remained constant and its value was approximately 0.1, which is 1/6 of Stainless3. The difference of μ' due to pitch p was approximately 15%.The reason why this error is occurred would be large deformation of the synthetic fiber rope which does not satisfy Coulomb friction model. Based on the derived value of $\mu' = 0.0919$ for the most appropriate groove shape, which was approximately 2.1 times higher than the original friction coefficient, we could calculate the required contact angle by using Eqn. (15) as $\theta = 348°$, in order to reduce the tension from 91.3% to 53.2% by using the figure-eight knot in Table I. In practice, it is desirable to introduce a safety factor for the terminal fixation strength. For example, adding one more turn reduces the tension to 34.2%, achieving the safety factor of 1.46. The pulley height increase is $p = 4mm$, which is relatively small compared with the pulley diameter.

Finally, we investigated the applicability of the optimum grooved pulley to different rope materials and different rope diameters. Figure 15 shows the strength efficiencies with the ropes made of UHPE, PBO, and Polyarylate fibers. Although Dyneema2 was slightly less than 90%, the other ropes successfully exhibited strength efficiencies larger than 90%. We
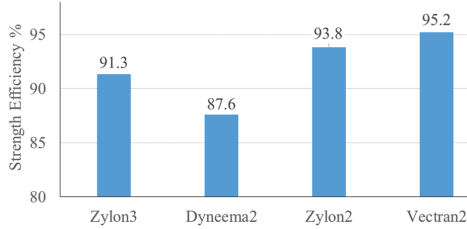
Fig. 15: Strength efficiencies of various material ropes
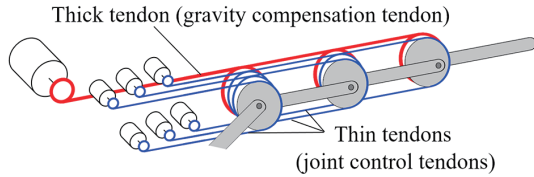
Fig. 16: Rope rooting of coupled tendon-driven mechanism with weight-compensation mechanism. The red thick rope pulled by a large actuator generated large torque in order to compensate for gravitational torque. The blue ropes pulled by relatively small actuators were used to control each joint.

Length [mm]	5700
Diameter [mm]	194
Arm Weight [kg]	28.3
Num. of D.O.F.	6
Rope Diameter [mm]	Gravity Compensation: $\phi5.5$
	Joint Control: $\phi1.5$
Rope Material	Gravity Compensation: Zylon
	Joint Control: Dyneema
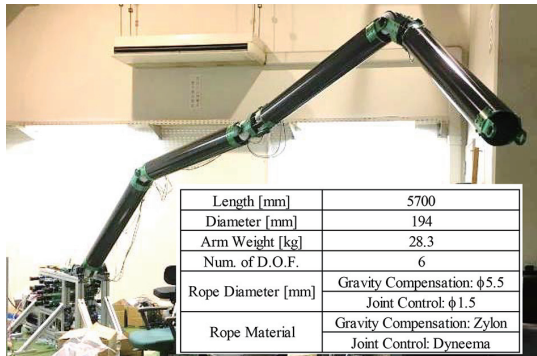
Fig. 17: Prototype model of coupled-tendon multi-joint manipulator "Super Dragon"

also tested Dyneema2 with $d = 1, 3mm$, and their strength efficiencies were 86.4% and 91.8%, respectively. These results suggest the generality of the grooved shape.

VI. EXAMPLE OF IMPLEMENTATION

This section briefly introduced implementation examples. A long-reach multi-joint manipulator was expected to be used for a decommissioning task in the Fukushima Daiichi Nuclear Power Plant. Due to the high dose level inside the Primary Containment Vessel (PCV), the size of the access hole was limited, whereas, the required length of the manipulator was larger than 9 m. To solve this extremely difficult design problem, we proposed a coupled-tendon multi-joint manipulator [6][17]. Schematic in Fig. 16 shows the tendon arrangement for a simplified three joint manipulator. To cope with a huge gravitational torque due to the very long configuration, a thick tendon named the gravity compensation tendon, was attached to the distal fixed pulley. The tendon was wound around passive pulleys in successive proximal joints, and pulled by a large output actuator. The thick tendon could roughly compensate for gravity torque by controlling the tension of the tendon depending on the posture of the manipulator. The residual gravity torque for each joint and individual joint angle were controlled by thin antagonistic pairs of tendons called the joint control tendon. (A more detailed mechanism and analysis can be found in [17]). Figure 17 shows a prototype model of the manipulator with a length of 5.7 m. All actuators were installed on the base unit, and each joint was controlled by synthetic fiber tendons, whose diameters were 1.5 mm. Furthermore, a thick synthetic fiber rope whose diameter was 5.5 mm, was installed and pulled by an air cylinder with a maximum output force of 21.1 kN. Figure 18(a) shows the terminal fixation of the joint control tendon on the distal fixed pulley. The groove shape had metric screw threads in order to reduce processing costs. Figure 18(b) shows the terminal fixation of the gravity compensation tendon. The groove shape was based on the most appropriate groove obtained in Section IV. Additionally, the overall size increased linearly such that it fit the thick rope. We confirm that the proposed fixation method successfully fixed the tendon under the maximum tension of 1.5 kN and 11 kN, for the joint control tendons and gravity compensation tendon, respectively.

VII. CONCLUSION

In this paper, we proposed a new length-adjustable compact fixation method for a synthetic fiber rope that achieves high
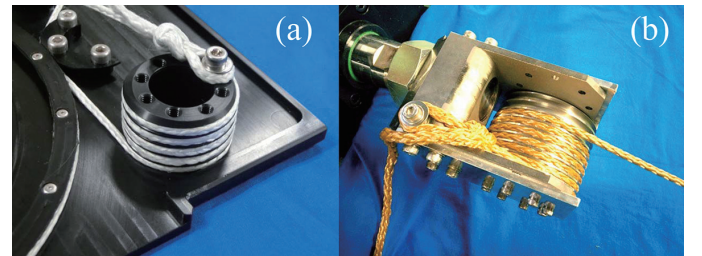
Fig. 18: Terminal fixation for (a) joint control tendon, and (b) gravity compensation tendon.